Report of the Committee to Compare the Scientific Cases for Two Gravitational-wave Detector Networks: (AHLV) Australia, Hanford, Livingston, VIRGO; and (HHLV) two detectors at Hanford, one at Livingston, and VIRGO

May 10, 2010

Table of Contents

Committee members:

Sam Finn	Pennsylvania State University
Peter Fritschel	LIGO-MIT
Sergey Klimenko	University of Florida at Gainesville
Fred Raab	LIGO-Hanford
B. Sathyaprakash	Cardiff University
Peter Saulson	Syracuse University
Rainer Weiss	LIGO-MIT (Chair)

Introduction:

The committee has compared the scientific merits of two gravitational-wave detector networks, HHLV and AHLV. HHLV consists of the proposed Advanced LIGO network of two 4km detectors at Hanford, Washington and one at Livingston, Louisiana coupled with the Advanced VIRGO, a French-Italian detector at Cascina, Italy. AHLV is a concept in which one of the Hanford detectors is moved to Australia. For modeling purposes we have assumed the location of the Australian detector is at Gingin near Perth, the site already developed by the Australian Collaboration. The orientation of the Australian detector relative to the others in the network has been considered a variable in the modeling.

The main emphasis of the study is to assess the scientific merits of the two networks in the epoch after the initial gravitational wave detections have been made and the field has become a regular branch of observational astrophysics. One can imagine such a situation after 2017. A secondary, though no less important, study is to establish the ability of a two and three element network to make the initial detections before 2017 while an Australian detector is being constructed. We were specifically asked *not* to make a recommendation for future action but to serve in a fact finding mode.

Although our primary charge is the comparison of the two networks, we also were asked to set the context for the comparison by imagining the field of gravitational wave astrophysics at the time when the networks would be operative. Some notions of the new astrophysical science from the advanced detectors and the development of the detectors are presented in the first two sections of the body of the report. This is followed by the main section of the report on the comparison of the networks in their ability to carry out the astrophysical program. That section is based on the studies done by and for the committee and is organized by scientific topic with each section divided into the results for compact binary coalescences (CBC) and unmodeled burst sources. A section on making the first detections ends the report. In an appendix, we give a brief description of the rationale for placing a 2km and a 4km detector at the Hanford site in initial LIGO and finally for completeness, present the committee charge.

Executive Summary of Results:

Ability to determine the position of a source in the sky: The AHLV network offers a significant improvement in establishing the sky location of gravitational wave sources with both modeled and unmodeled waveforms (time series). Depending on signal to noise and the location on the sky, the ratio of the uncertainties in the position of a source can be 5 to 10 times smaller for the AHLV than for the HHLV network. In many places on the sky, using reasonable signal to noise, the uncertainty in position approaches 1 degree; sufficiently small to enable electromagnetic astronomical identification of the source. Furthermore, the shape of the uncertainty contours on the sky are closer to being circular rather than elongated. Both factors are critical for the epoch once detections have become common place, enabling gravitational wave observations to become a branch of astrophysics and cosmology.

Source parameter estimation and waveform reconstruction: The AHLV network offers some improvement over HHLV in determining the physical parameters at the source. The study has been done primarily for the NS/NS coalescence sources in which degeneracies in the fitting matrices are resolved by the AHLV network. One dramatic example is the ability to separate the solution for the source distance and the source inclination of the orbit relative to the observer. Another study has shown improvement in determining the polarization of the gravitational wave at the Earth with the AHLV network. The improvement in part comes from the possibility of choosing an optimum orientation for the Australian detector. The ability to "reconstruct" arbitrary waveforms was also investigated. In this as well, the AHLV network is able to infer the waveform of an incident burst with significantly smaller uncertainty.

Network sensitivity and false detection probability: For a specific astrophysical source, the sensitivity, the minimum amplitude gravitational wave signal one can detect, depends primarily on the noise spectrum of the detectors and the probability distribution of the noise. For equal detectors in a network, the sensitivity improves with the reciprocal square root of the number of detectors. Our study shows little difference between the gravitational wave sensitivity of the HHLV and AHLV networks.

An important finding is that the false detection probabilities vs threshold signal to noise for unmodeled bursts in the two networks are not greatly different with non-Gaussian data and become almost the same for data that has been reduced to Gaussian statistics. The conclusion comes from using algorithms that trade on the coherence of the waveforms in the different detectors and the improved ability to determine the sky position in the AHLV network. The false alarm probability for modeled sources, such as chirp waveforms from binary neutron star coalescences, may not be the same for the two networks when using the *currently* developed detection algorithms. These algorithms filter the data with chirp templates and then search for coincidence between the detectors after the filtering. The sky position information is not used directly to establish consistency although one could use the data streams from collocated detectors to provide a veto independent of source sky position and polarization. Algorithms for modeled sources that coherently detect the chirps in the different detectors and solve for the sky position *need to be incorporated into the VIRGO/LIGO analysis pipeline*. With such improved analyses, the false detection rates for the two networks are expected to be comparable.

Environmental correlation between detectors : The AHLV network does not suffer from local correlated environmental perturbations while the HHLV network is vulnerable to them. The gravitational wave search for all classes of sources is disturbed by these correlations; most affected is the search for a stochastic background of gravitational waves both from cosmological and unresolved "foreground" sources. Here it is worth noting that with the improvements in the low frequency performance of the advanced detectors, the overlap of the responses to an isotropic background of stochastic gravitational waves will be larger for widely separated detectors than it was for the initial detectors.

A factor of a different nature than those given earlier, favoring the AHLV over the HHLV network, is the reduction in the risk of failure and probability of increased duty cycle when two of the network detectors are no longer situated at the same location.

Detection of compact binary sources before an Australian detector would be available : A question that arose early in the committee and in the Collaboration was whether making a decision to move one Advanced LIGO detector to an Australian site would preclude the ability to make detections of known gravitational wave sources early in the Advanced detector era. In particular, would it still be possible to make a detection of NS/NS binary coalescences with HLV or at worst a detector pair such as HL. A significant result of the studies done for the committee was the finding that with a new detection statistic that weighs the signal-to-noise with how closely the data matches the expected chirp waveform and the application of the same type of vetoes as in prior science runs, it was possible to approach Gaussian statistics despite the non-Gaussian noise in the detectors. For a chirp amplitude signal to noise (SNR) of 8 in a single detector, it is possible to achieve an accidental detection rate with a pair of detectors less than 1/30 years and correspondingly even lower rates with three detectors.

Committee Mechanics:

The committee met 15 times by telephone and had one face to face meeting. Early on the committee interviewed chairs and chair designees of all the VIRGO/LIGO Scientific Collaboration data analysis search groups. We asked the following questions:

A) What might be the situation in the field of gravitational wave astrophysics after 2017?

B) How to respond both in observing programs and in incremental improvements of the detectors to the discoveries that have been made?

C) How well would the two alternative networks:
   1) determine position on the sky,
   2) determine the gravitational wave time series and the polarization,
   3) determine the parameters of the source (mass, spin, inclination, distance...),
   4) determine source statistics and populations?

D) Is there an advantage for either network to make the first detection?

It is worth noting that in our interviews there was universal agreement concerning the scientific value of the AHLV over the HHLV network. The primary concerns were about logistics and timing associated with moving one of the Advanced LIGO detectors to Australia. It became clear that by charging our committee to analyze only the scientific case, we were given the easy job.

Notes of the meetings and the interviews are kept on the committee website: https://gwastro.psu.edu/wiki/LIGOSouth/index.php?title=LIGO_South

Scientific strategies after the first detections

We considered the choices that might confront us after the first GW detections are made and how the location of a third LIGO interferometer might interact with these choices. Since the differential volume of space is greatest near the limits of detection for any source, we expect that most signals detected in the early post-discovery phase will have low signal to noise.

We expect that the first detections will be transient sources. These may very well be compact binary coalescences, but both burst and CBC search techniques will be important in uncovering the physics. We expect such sources will dominate detections in the years following the first discoveries. However, we must maintain vigilance for periodic and stochastic sources as well during these years. We frame the discussion below in three distinct stages:
- a first discoveries stage that will cover the first few published detections;
- an astronomical census and population modeling stage
- a stage targeting new classes of sources.

First-Discoveries Stage In the first discoveries stage, the emphasis will be to identify as accurately as possible the nature of each source and to exploit the first discoveries to test General Relativity under strong-field conditions. Recovery of waveform information in both polarizations will be the primary concern. However, it should be noted that sky location and event time will likely be essential elements of detection confidence, for cases in which an electromagnetic signal is associated with the event.

Astronomical Census and Population Modeling Stage After the first 3 or 4 detections are made from a class of sources, attention likely will shift to statistical astronomy, based on measuring the spatial distribution of the events and trying to identify the source populations and the history of the progenitors behind the GW signals. Waveform information from both polarizations will still be important, but sky localization will be essential to identify host galaxies and to look for statistical trends among a number of detected sources. The history of gamma-ray astronomy with BATSE aboard the Compton Gamma-Ray Telescope is a good analogy for this important stage of GW astronomy. The most compact error ellipses on the sky – as parameterized by area and ellipticity – will yield the best science outcomes during this stage.

Targeting New Classes of Sources Once the number of detected sources in a given class is measured in the dozens, trading off sensitivity to an already detectable class of signals in favor of optimizing detector characteristics for an as yet undiscovered class of sources is a reasonable strategy. For example, one might tailor the response of one or more interferometers to optimize sensitivity to a compact binary inspiral endpoint or to an LMXB, such as Sco-X1.

Incremental Improvements to Advanced LIGO

The observing program associated with Advanced LIGO, both during its construction and in the years following, is more varied than that of initial and enhanced LIGO and is expected to be driven by the discoveries that are made. The range of observations and

optimizations that can be performed is important in considering and designing a new observing program which includes a sensitive detector in Australia. We consider here some of the possibilities and the technical developments being considered.

The Advanced LIGO detectors will be brought into operation much in the same manner as the initial detectors were, with periods of commissioning followed by short engineering and science runs. **Figure 1** shows a set of operating modes for the Advanced Detector.
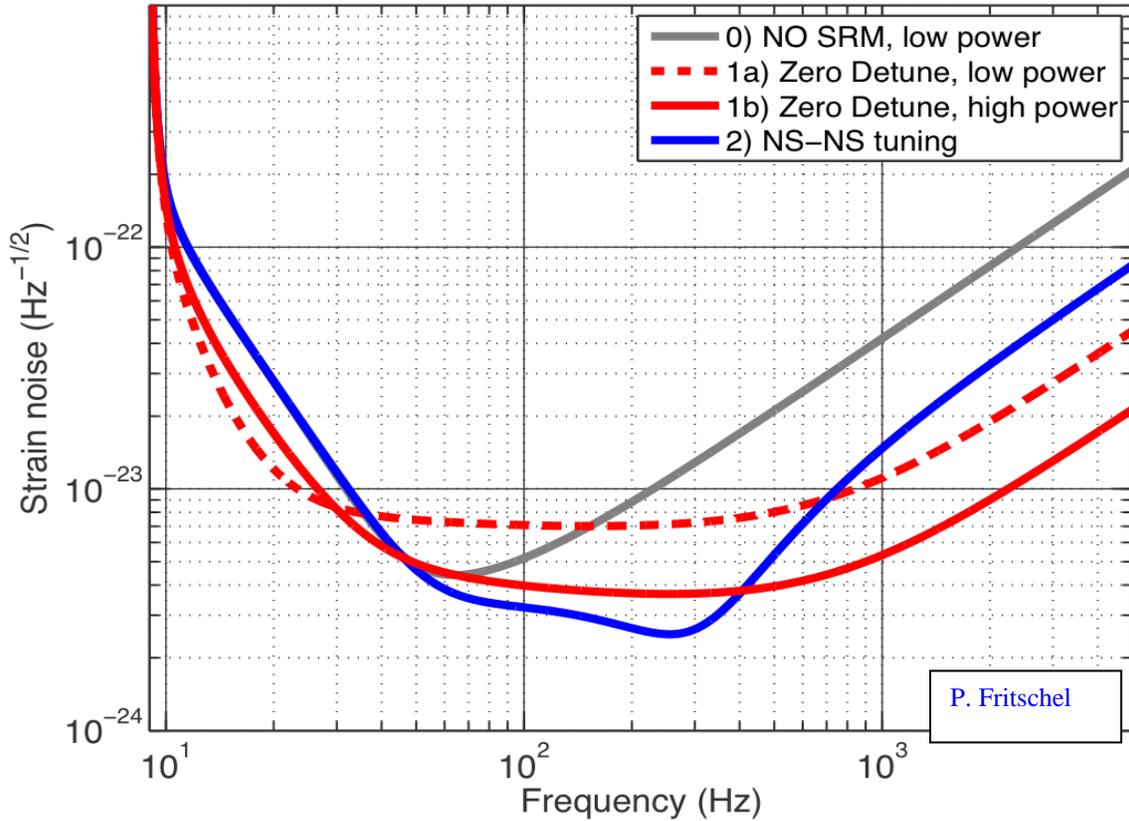
Figure 1 Different modes of operation for the Advanced LIGO Detectors

Mode	NS-NS Range	BH-BH Range	P_{in}	T_{SRM}	ϕ_{SRC}	h_{RMS}, 10^{-22} (band)
0	150 Mpc	1.60 Gpc	25 W	100%	–	0.53 $(40-140\,\mathrm{Hz})$
1a	145 Mpc	1.65 Gpc	25 W	20%	0 deg.	0.70 $(110-210\,\mathrm{Hz})$
1b	190 Mpc	1.85 Gpc	125 W	20%	0 deg.	0.37 $(205-305\,\mathrm{Hz})$
2	200 Mpc	1.65 Gpc	125 W	20%	16 deg.	0.25 $(205-305\,\mathrm{Hz})$

Table 1 Parameters for the different modes. The NS/NS and BH/BH range is for one detector with source location averaged over the sky and averaged over polarization. Power in is measured at the input to the power recycling mirror. T_{SRM} is the transmission of the signal recycling mirror and ϕ_{SRC} is the phase shift of the carrier after a round trip in the amplitude recycling cavity. Figure and table come from "Advanced LIGO Systems Design" LIGO T1010075-V2, P. Fritschel, editor, 09/18/2009.

The modes are associated with different configurations of the instrument as well as different parameters and tunings, see **Table 1**. Early in the Advanced LIGO development,

once the new seismic isolation and suspensions have been installed, it will be possible to make a run in mode "0". This mode has a reasonable probability of being able to detect NS/NS binary coalescences at rates as great as a few per month.

The formal Advanced LIGO construction project incorporates the full set of improvements consisting of the new seismic isolation systems, new suspensions, higher power laser and the inclusion of a signal recycling mirror. Developmental research is now being carried out to enable incremental improvements in the Advanced Detector in response to astrophysical observations or to improve the depth of the searches. Current research includes the following programs.

Non-invasive incremental improvements
Regression of Newtonian gravitational gradients : The concept is to use external seismometers and tilt sensors to measure the seismic compression and expansion of the ground leading to the fluctuating Newtonian gravitational gradients on the interferometer test masses and then with this information to remove the perturbing forces. The idea in a primitive form is now being used in enhanced LIGO to significantly reduce the dynamic range of the interferometric control systems against seismic excitations. In Advanced LIGO the scheme will improve the low frequency sensitivity of the instrument and may extend the search for BH/BH binaries below the 10Hz region where Newtonian gravitational gradient noise begins to compromise the performance.

Application of "squeezed" light to the Advanced LIGO detector : The ability to use ""squeezed" light injected at the antisymmetric port of the interferometer to reduce the phase noise of the interferometer is being developed in several laboratories around the world. In LIGO, a demonstration and development experiment will be mounted between the end of the enhanced LIGO program and the full deployment of Advanced LIGO. The experiment is designed to establish the ability to reduce the phase noise at hundreds of Hz up to several kHz while not destroying the performance at lower frequencies. The application of "squeezed" light is not in the current Advanced LIGO program but is being considered as a moderately non-invasive incremental improvement. The observational improvements will occur in the several hundred to several kHz region of the spectrum which includes the end point of NS/NS coalescences and significant energy in the gravitational wave spectrum of supernova models. "Squeezed" light will also offer a hedge to improve the phase noise if operation at high power proves to be troublesome.

Invasive incremental improvements
Lower frequency vertical modes for the fused silica suspensions : The coupling of thermal noise of the vertical suspension to the horizontal motions of the test mass comes about because of the curvature of the Earth. The test mass suspensions at the two ends of the 4km arms do not hang parallel. The amount of vertical thermal noise projected into the horizontal (the sensitive axis) can be reduced by lowering the resonance frequency of the vertical suspensions. This can be accomplished by using more compliant vertical support springs in the new suspensions. The interferometer sensitivity improvements would be at frequencies below 150Hz.

Variable reflectivity signal recycling mirror : The signal recycling mirror for the currently designed Advanced LIGO interferometer has a fixed reflectivity so that operating in the various modes shown in Figure 1 would require opening the apparatus and replacing the mirror. It is also possible to make a variable reflectivity signal recycling mirror by using a cavity which could be tuned while in place in the interferometer. This is one example of being able to tune the spectral response of the instrument by varying parameters in situ and will become part of the standard operations in the epoch when gravitational wave detections are common place.

Larger spot size on mirrors : The contribution of mirror coating thermal noise is reduced by increasing the light beam spot size on the test masses. The reduction in the noise comes about by taking larger averages over the mirror surface and is most important in the spectral region around 100 Hz, the critical region for NS/NS binary coalescences. Various types of beam wavefronts have been modeled in optical propagation programs which exhibit larger spot sizes without significant increase in the diffraction loss. The application of such beams will require repolishing and recoating some of the optics in the interferometer.

Comparison of the two networks

Modeling to answer a variety of questions was carried out for the committee by several groups. B. Sathyaprakash guided a group[1] which studied the issues for modeled sources, in particular, for binary neutron stars and low mass BH binary systems. The results given here are for a pair of $1.4\,M_o$ neutron stars. They have looked at two versions of the Australian network AHLV with the orientation along the current planning at Gingin and A_{45}HLV rotated by 45 degrees.

Another group[2] guided by Sergey Klimenko studied the networks for the detection of unmodeled sources using the coherent burst algorithm. Modeling for waveform reconstruction was done by Sam Finn. The results of the modeling are gathered together in this section of the report under a set of common headings. The individual groups will publish their more extensive results separately. The results below are presented separately for modeled and unmodeled sources.

The light travel time between various detectors is given in **Table 2**.

Table 2 Light travel time between various detectors in milliseconds

Detector	AH	AL	AV	HH	HL	HV	LV
Distance	39.3	41.6	37.0	0.0	10.0	27.3	26.4

Antenna Patterns and Network Sensitivity
Modeled sources (compact binary systems)

A primary question concerning the various networks is their detectability of sources and their sky coverage. These two questions were addressed by looking at the combined antenna patterns of the various networks. **Figure 2** compares the joint antenna patterns of networks HHLV, AHLV and A_{45}HLV. The three networks have all similar joint antenna patterns, with A_{45}HLV showing a slightly improved sky coverage. We computed the average reach of each of these networks for a sample of three different binaries. We posed the question of sky coverage by computing the total area of the antenna pattern at 50% of the average sensitivity. The results are shown in **Table 3**. We see that there is not much difference in the range of these networks nor their sky coverage. We have confirmed these analytical calculations by a large scale Monte-Carlo simulation.

---

[1] Steve Fairhurst, B.S. Sathyaprakash, P.J. Sutton, John Veitch (Cardiff University), Ben Farr, Vivien Raymond, Ilya Mandel, Vicky Kalogera, Marc van der Sluys (Northwestern University), Sukanta Bose (University of Washington)

[2] Sergey Klimenko (University of Florida at Gainesville), G.Vedovato. INFN, Padova, Italy, M.Drago, University of Padova, Padova, Italy , V.Re, Trento University, Trento, Italy, I.Yakushin, LLO.
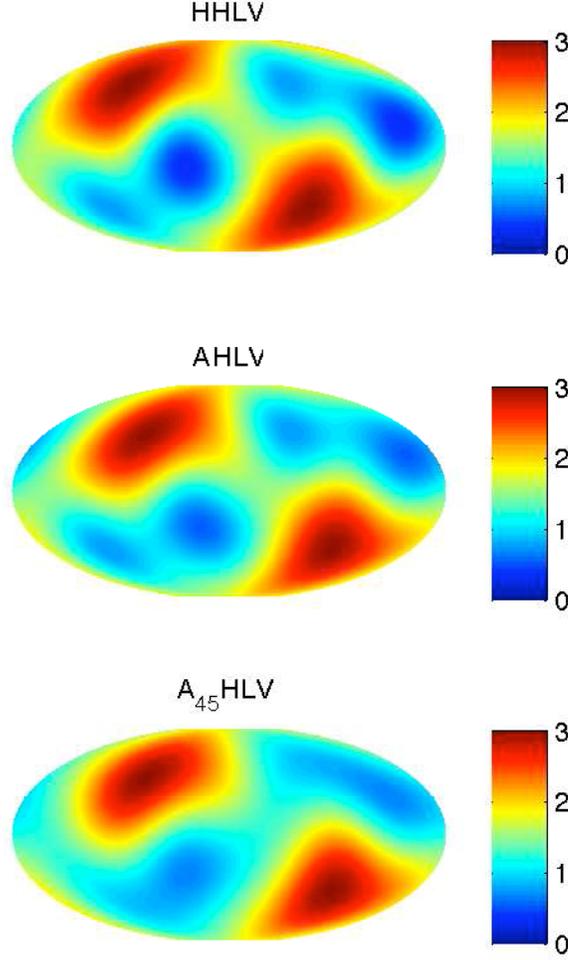
Figure 2 Joint antenna pattern of HHLV, AHLV and A$_{45}$HLV networks. The color coding indicates the detected energy in the sum of the polarizations. The maximum value is 4 for an optimally located and oriented source. The change in blue area between the networks is worth noting.

Network \ Source	(1.4, 1.4) M$_o$	(1.4, 5) M$_o$	(1.4, 10) M$_o$	Sky Coverage
HHLV	259.3 ± 0.2 Mpc	427.0 ± 0.5 Mpc	548.3 ± 0.7 Mpc	50.4%
AHLV	259.7 ± 0.4 Mpc	427.2 ± 0.7 Mpc	549.0 ± 0.8 Mpc	48.6%

Table 3 The reach is computed by demanding that the network SNR is 12 and at least two detectors have an SNR of 6 or more. The last column gives the fractional area of the sky for which the antenna response $F^2 = F_+{}^2 + F_x{}^2$ is more than half of the maximum response. Note: the distances are given in terms of the horizon distance for an optimally polarized source and are larger than the averaged distances used in **Table 1** by a factor of 2.8. The average distances are used by the experimenters and the horizon distances by the modelers.
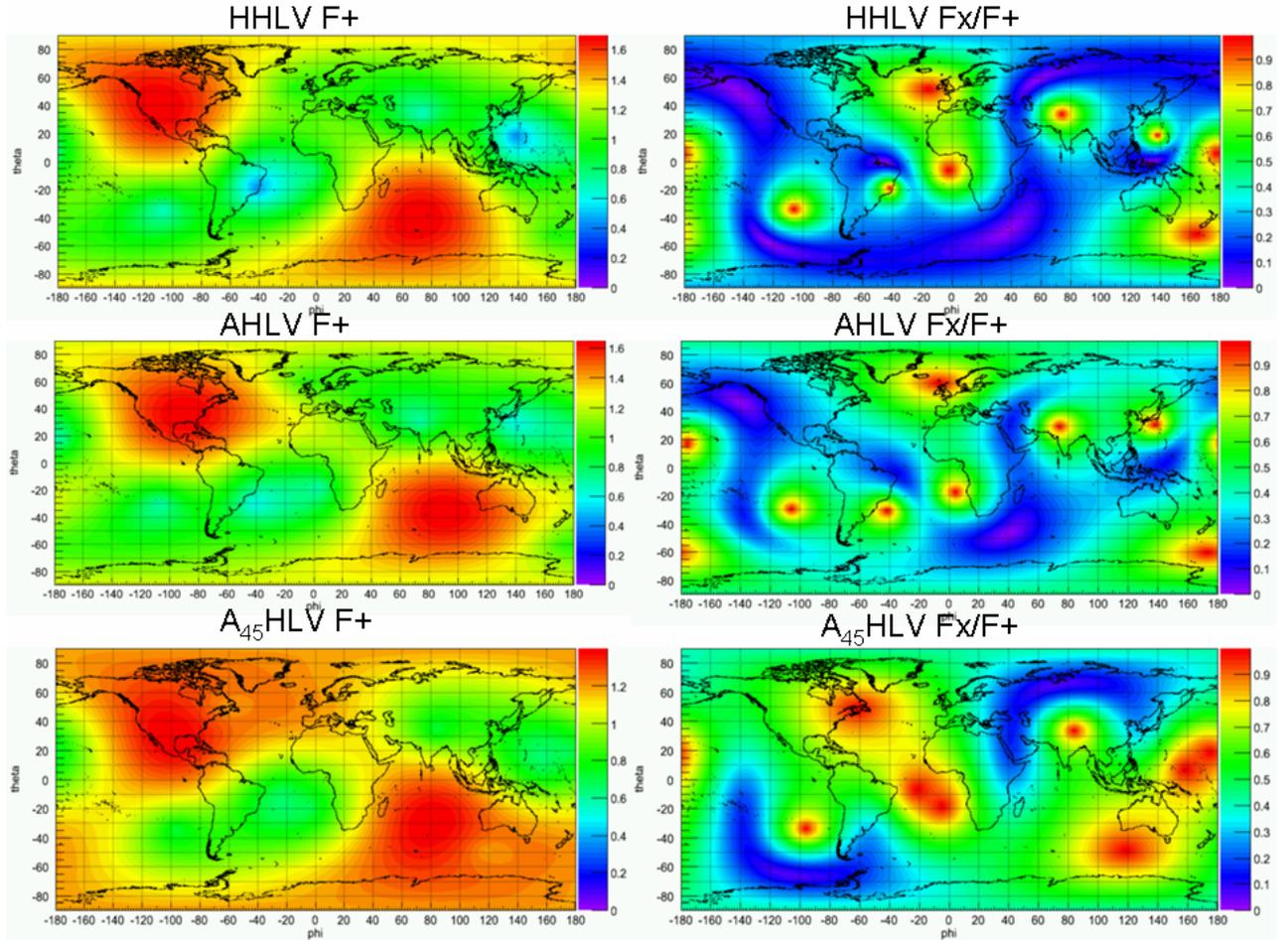
Figure 3 Comparison of network sensitivity for gravitational waves with equal amplitude of the polarization at the source. The plot shows the sensitivity of the networks for the magnitude of the dominant detected polarization, F+ (left), and the ratio of magnitudes of the Fx/F+ (right) for unmodeled burst sources as a function of sky coordinates.

The norms of the antenna pattern vectors $|F_+|$ and $|F_\times|$ characterize the network sensitivity to the GW polarizations. Closely aligned networks (like HHL) have poor sensitivity to the second polarization: $|F_+| >> |F_\times|$ which makes full reconstruction of the GW signal difficult. **Figure 3** show the $|F_+|$ and the ratio $|F_\times|/|F_+|$ for HHLV, AHLV and A_{45}HLV networks. The ratio $|F_x|/|F_+|$ gives the ratio of the SNRs produced by each gravitational wave component assuming equal amplitude in each polarization at the source. The red spots on the $|F_x|/|F_+|$ plots indicate the network has equal sensitivity for both gravitational wave components. The blue spots indicate that the smaller gravitational wave component is not measurable for a moderate SNR (a network SNR < 30).

Another study of the ability to determine the polarization of the gravitational waves from the two networks was carried out with the intent of evaluating waveform reconstruction.
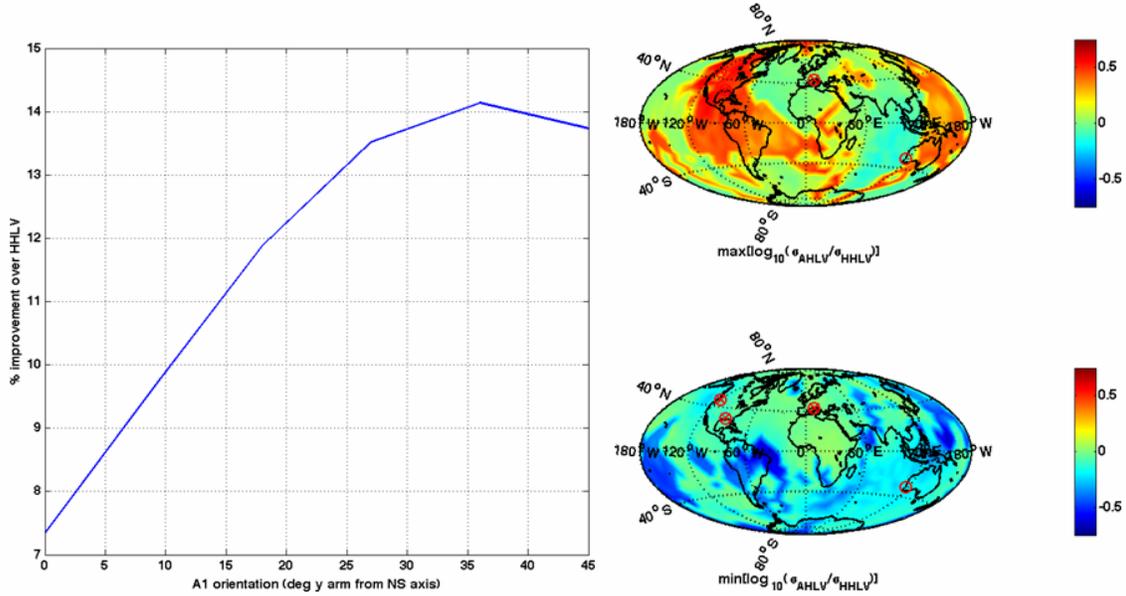
Figure 4 The ability of the AHLV relative to the HHLV network to determine the polarization of burst sources distributed over the sky. At each location in the map the source is overhead and has equal polarization components. The left plot shows the improvement of AHLV relative to HHLV averaged over the sky as a function of the orientation of the Australian detector. The plots on the right show the (log) ratio of the statistical uncertainty in the recovered waveform. The two plots show different extremes; in the upper plot the ratio for the source orientation that most favors HHLV is shown; in the lower plot the source orientation that most favors AHLV is shown. Nowhere over the sky is HHLV significantly more sensitive than AHLV and, over large parts of the sky, AHLV is more sensitive than HHLV.

To identify the incident strain requires an antenna array whose elements are sufficiently independent in their response to permit the inference of the radiation "field" incident on the ensemble. Correspondingly, the AHLV and HHLV antenna arrays will be different in their ability to infer **h** from observations **d**.

Finn & Lommen (2010) describe how to infer an arbitrary **h** from antenna array observations **d**. The result of this analysis may be summarized as

$\mathbf{h} = (h^0_+ \pm \sigma_+)\mathbf{e}_+ + (h^0_x \pm \sigma_x)\,\mathbf{e}_x$, where h^0_+, h^0_x, σ_+, and σ_x are all functions of the antenna array observations **d**, the array element noise power (cross)spectral densities, array element response functions, and wave propagation direction. The σ are understood to describe the 68% probability bounds.

To investigate the relative ability of the AHLV and HHLV antenna arrays to infer the waveforms of an arbitrary source we have simulated antenna array datasets (signal + noise) and applied the Finn & Lommen analysis to them. Varying source orientation and location on the sky, but holding all else fixed, we find that median sensitivity of the AHLV network is superior to the HHLV network: i.e., the median of $(\sigma_+ \sigma_x)^{1/2}$ over all source orientations, is smaller for AHLV than for HHLV. The advantage varies with

12

source amplitude and AHLV orientation. The best advantage corresponds to AHLV oriented with arms ~+36 deg from the NS and EW axes. Preliminary investigations indicate that for this orientation the error bars may be 15% smaller for AHLV than for HHLV. Figure 4 shows the principal results of the analysis of the two networks.

A measure of the sensitivity of the networks is provided by the search volume, the volume of space defined by enclosing an isotropic distribution of equal strength sources at the network limiting sensitivity. The useful quantity is the ratio of the volumes for different networks as this becomes independent of the search algorithm and the nature of the source. **Table 4** shows the volume ratios for a variety of networks with respect to the HHL network. The calculations assume the SNR thresholds are the same for all the networks. The table also shows the reduction in effective search volume, and thereby increases in the SNR needed for detection, due to non-stationary and non-Gaussian noise in the detectors. The excess noise causes extended non-Gaussian tails in the estimates for the false alarm rates as a function of SNR (see **Figure 11**).

Network	V ratio Gaussian noise	V ratio FAR < 1/5 y
HHL	1	0.22
HL	0.54	0.05
HLV	0.93	0.32
HHLV	1.44	0.74
A_{45}HLV	1.43	0.51

Table 4 Network search volume ratios relative to the ideal HHL network. The second column shows the volume ratios assuming Gaussian noise for all networks. The third column shows degradation of the search volume due to non-Gaussian and non-stationary noise. The calculation was made over the full 64 to 2048Hz band in the S5/S6 runs . The low frequencies are the major source of the non-Gaussianity.

Determination of Source Sky Position
Modeled Sources
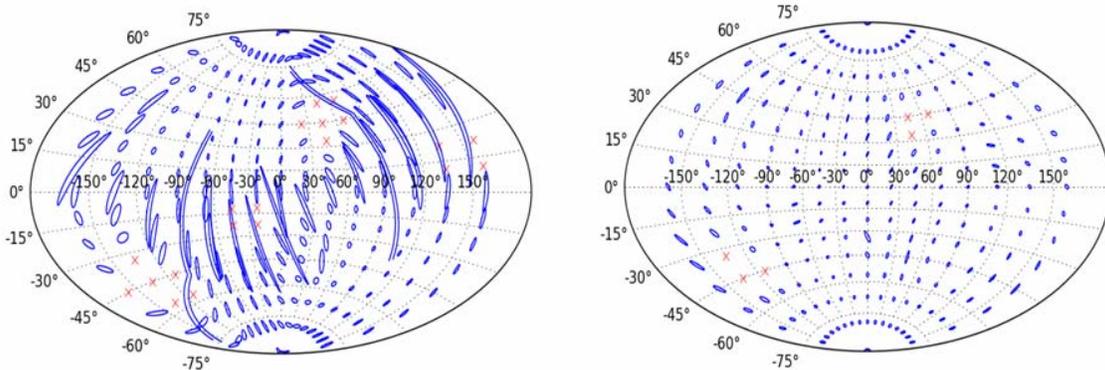
Figure 5   Left: Sky localization with the HHLV network. Right: Sky localization with the AHLV network. The plots show the 90% confidence contours for binary NS sources face on and at a horizon distance of 200Mpc. The plot assumes that the advanced detectors would achieve a SNR =8 for these sources at a horizon distance of 180Mpc. The red X's are points in the sky where the signal would be poorly detected with a network combined SNR < 12 .

For a three-site network, one can only constrain the location of the source within the plane of the detectors. This gives the well-known degeneracy in localization, giving two sky patches one above and one below the detectors. In what follows, we will assume that this degeneracy can be broken by considerations of the relative observed amplitudes. In reality, however, this will not always be possible. In the case of three detectors, the best case scenario has the source overhead the plane of the detectors. The worst case is with the source in the plane of the detectors. For the four-site network, the sky-localization degeneracy is broken. Furthermore, there is no longer a particularly bad sky location.

In this study, we use only the timing of binary neutron star coalescences to triangulate a source on the sky. In the case of Advanced LIGO, the time of arrival of a signal can be determined to within 0.13 ms for a signal that produces an SNR of 10. A Monte Carlo with 1,000,000 potential sources distributed uniformly in the sky, uniform in volume, and with a uniform orientation distribution was performed. A source is said to be *found* by requiring that:

1. the combined (root sum square) SNR was at least 12, and

2. the SNR in at least two detectors was 6 or more.

Table 5 compares the detection ability and sky localization of a three-site network with a four-site network. For both 3- and 4-detector networks, the number of sources found by the network containing a detector in Australia is the same as the one without it. However, as expected, sky localization improves significantly in a network that contains an Australian detector. For example, in the case of a four-detector network, the AHLV network localizes four times as many sources within 5 sq deg as does the HHLV network. The better sky localization of an AHLV network means that it is necessary to survey a volume that is a factor 3 to 4 smaller than in a network that doesn't include the Australian network.

Network	Fraction found	5 deg^2	10 deg^2	20 deg^2
ALV/HLV	1.04	3.4	2.0	1.3
AHLV/HHLV	1.03	4.1	2.6	1.7

Table 5 Comparison of HLV vs ALV and HHLV vs AHLV with regard to number of found sources, fraction of sources with 90% confidence sky-localization to better than 5, 10 and 20 square degrees.

One of the important goals for gravitational astronomy is to be able to follow-up potential events with astronomical telescopes. Observing events with optical, radio, X-ray and other EM telescopes can give further information that is very crucial to the scientific payoffs. For example, by measuring the red-shift of the host galaxy of a binary neutron star merger (which would require optical observations) it would be possible to confirm the Hubble flow and make measurement of the Hubble parameter that is completely independent of the cosmic distance ladder. This is because, inspiraling binaries are *self-calibrating standard candles*, that allow a very precise measurement of their luminosity

distance from a knowledge of their gravitational wave amplitude in three or more detectors.

An important question in relation to follow-up is not only the size of the sky-localization error ellipses but also their shape. **Figure 5** shows 90% confidence sky-localization error ellipses for binary neutron star mergers at 200 Mpc whose orbit is face-on with respect to the line-of-sight. The left panel corresponds to a three-site HLV network and the right panel corresponds to a four-site AHLV network. The error ellipses are pretty elongated for sources that are roughly in the plane of the three-site network (left panel) and they get significantly smaller and more rounded in the four-site AHLV network.
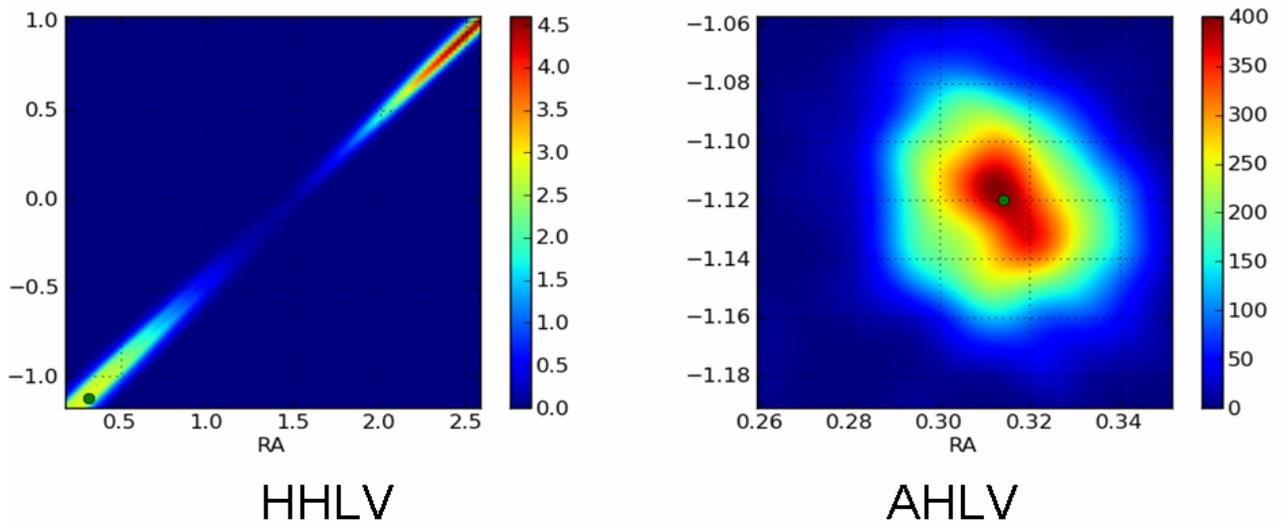
Figure 6 Examples of the sky localization contours in the two networks. The green dot shows the true position of the source in the modeling. The color coding indicates the probability density in units of 1/steradian

Figure 6 presents another comparison of the relative ability of the two networks to determine a source location on the sky. The probability distribution for the sky position is shown as part of the multi-parameter fits for the modeling of NS/NS coalescences . The modeling is described later in this document. The green dot is the injected position of the source. The HHLV network suffers a degeneracy in the sky position which is resolved in the AHLV network. Furthermore, the AHLV network provides uncertainty contours that are more circular and smaller.

Unmodeled sources
The coordinate reconstruction depends on the signal waveforms, polarization content, characteristic frequency and constraints used for the reconstruction. In this study we consider the least constrained case of burst searches (un-modeled all-sky search) used for reconstruction of 10 different ad-hoc GW signals uniformly distributed over the sky.

Figure 7 shows the reconstructed error angles (averaged over the sky) as a function of SNR. In general the pointing performance is increased with the SNR, but as shown on the 90% confidence plot, for the HHLV network a significant fraction of even high SNR events is not well reconstructed.
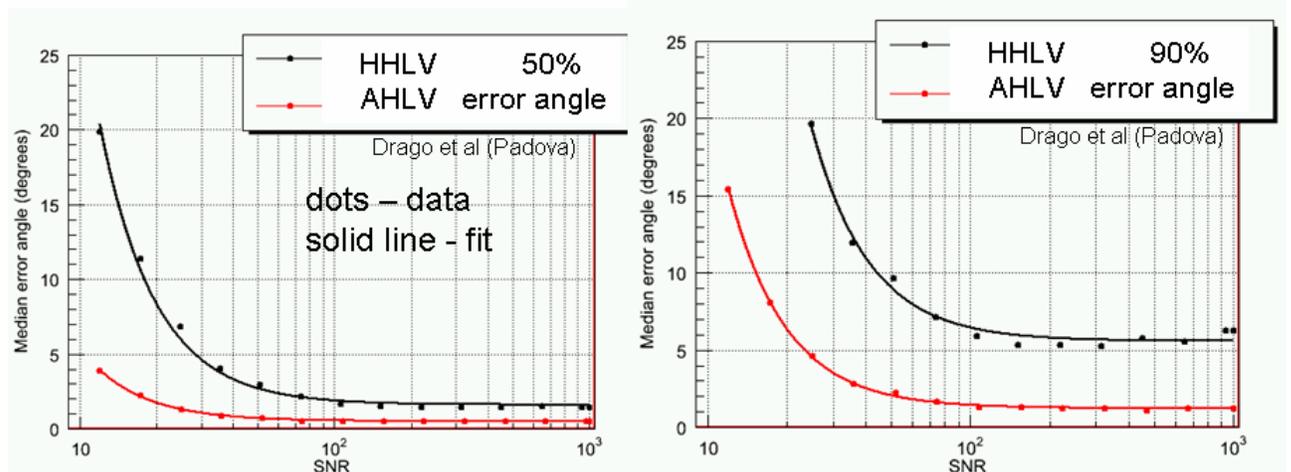
Figure 7 Error angles in degrees for 50% (left) and 90% (right) confidence as a function of the network SNR.

Figure 8 shows pointing capabilities of both networks as a function of sky coordinates. It shows the average median error angle for events with SNR < 30. These plots show that for expected low SNR signals the 4-site $A_{45}HLV$ network has significantly better pointing performance than the HHLV network. The improvement is due to the two main effects:

- The pointing is based on the triangulation and the HHLV network has zero redundancy. In many cases due to a particular polarization content of the signal or un-favorable sky location one detector may drop out of the measurement effectively reducing the network to two sites. The AHLV network is more robust if one detector is lost from the reconstruction.
- In many cases (particularly for un-modeled burst searches) the HHLV network can not resolve the actual-mirror location degeneracy which results in larger error regions. There is no such degeneracy for the AHLV network.

Another advantage of the AHLV network is that the coordinate reconstruction is much less affected by calibration errors.
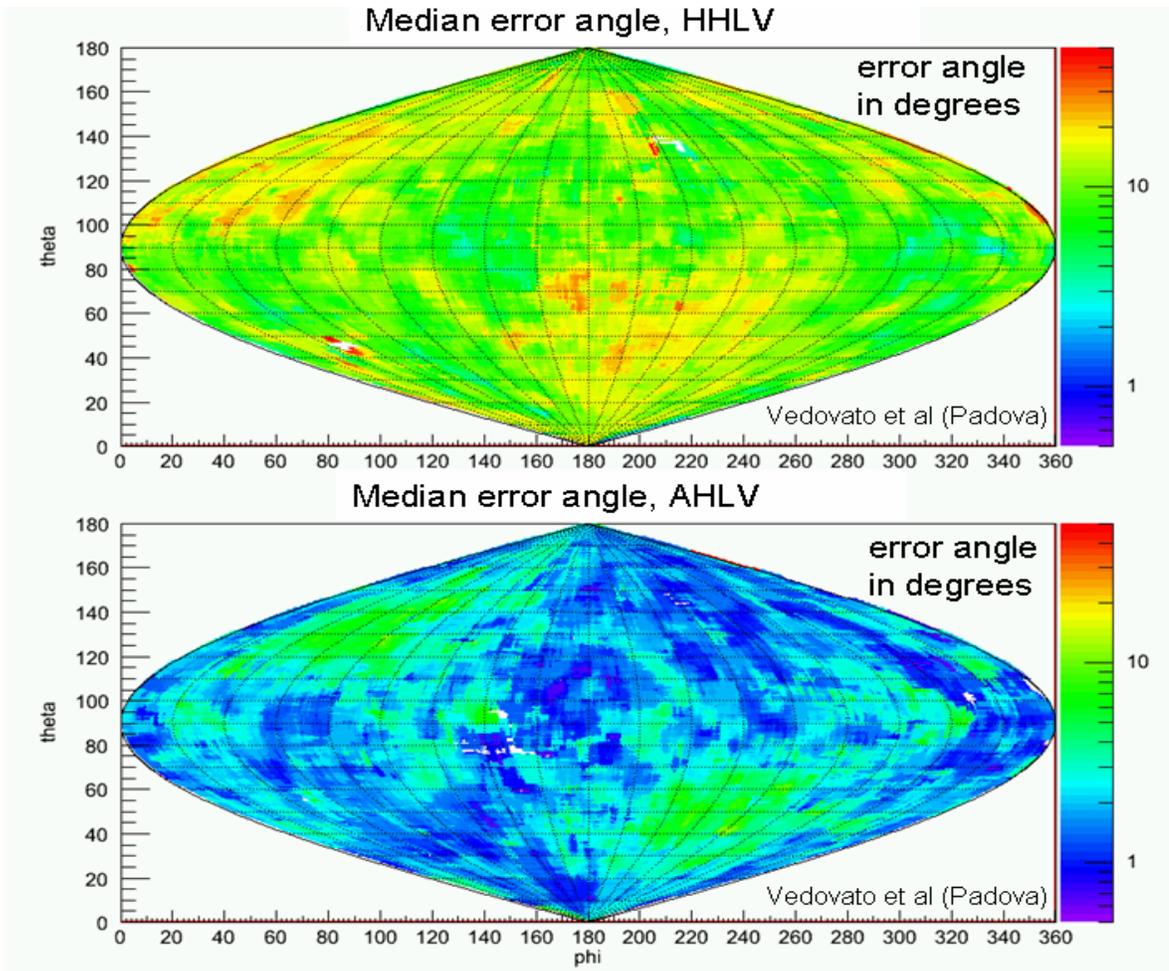
Figure 8 Average error angle as a function of sky coordinates for the two networks.

Source Parameter Estimation

Modeled sources

Parameter estimation studies based on arrival times neglect the correlations among different parameters that are known to exist in the case of binary inspiral signals. We have, therefore, used Bayesian methods to characterize the posterior probability density function of all the signal parameters. We assumed our source to consist of a pair of non-spinning neutron stars on a quasi-circular orbit. In this approximation, the source is characterized by nine parameters: Luminosity distance D_L, sky location, θ, ϕ, polarization angle ψ source inclination ι, the masses M, η, epoch of coalescence t_C and phase at that epoch ϕ_C.

Table 6 compares the performance of the two networks, averaged over 625 different sky locations, polarizations and inclinations, in terms of the area of the sky to which an individual source can be localized to within 67%, 90% and 95% confidence intervals. We have also listed the fractional error in the measurement of the luminosity distance $\Delta d_L/d_L$. At 90% confidence interval the AHLV network resolves a source a factor of 2 to 3 better than the HHLV network. However, the estimation of the luminosity distance remains unchanged.

17

Network	67% confidence deg^2	90% confidence deg^2	95% confidence deg^2	$\Delta d_L/d_L$
HHLV	16.6	29.4	33.9	0.15
AHLV	8.1	15.2	17.7	0.18
A$_{45}$HLV	7.4	13.4	15.8	0.14

Table 6 The mean resolution of each network in square degrees, averaged over RA, dec, ι and ϕ.

The most important advantage of the AHLV network is its ability to break the degeneracy of the source location that we mentioned before. As another example of the advantage of a four-site network, let us look at the degeneracy between inclination angle and luminosity distance. A three-site network does not have the ability to resolve these variables uniquely, especially for edge-on binaries. In **Figure 9** we have plotted the two-dimensional probability distribution function for a source at $(D, \iota) = (180\ \text{Mpc}, 1.68\text{rad})$. The HHLV network obtains a bimodal distribution for these two variables while the AHLV network shows a unimodal distribution and the degeneracy seen in HHLV is broken.

A second MCMC study was performed in order to confirm the results. This uses an independent code and a somewhat different algorithm to compute the posterior distribution. An agreement between the two approaches will be a useful way of confirming the overall results.

Veitch et al (Cardiff)

HHLV   AHLV
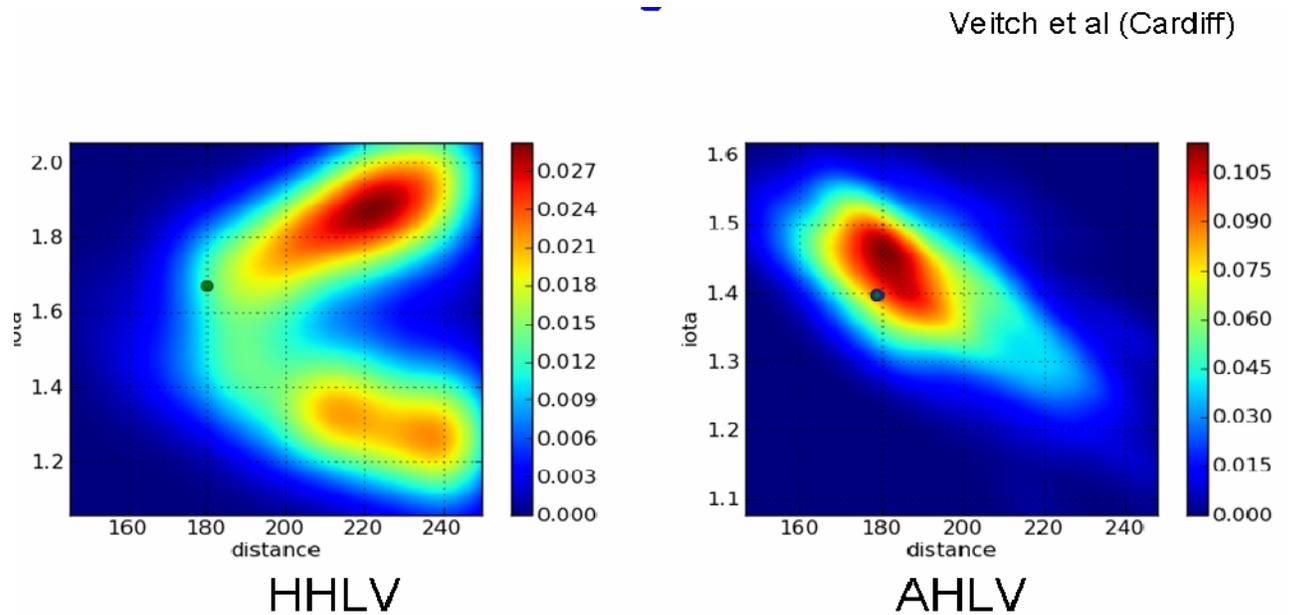
Figure 9 Two dimensional probability density contours for the model parameters of a binary neutron star system's luminosity distance and orbital inclination angle relative to the line of site in the two networks. The green dot shows the input value of the model parameter (iota is symmetric about π). The solution using the HHLV network is bimodal. The degeneracy is broken in the AHLV network. The color coding indicates the amplitude of the probability density in units of 1/(Mpc*radian).

Table 7 lists 2 - σ confidence intervals for the AHLV and the A$_{45}$HLV network configurations as fractions of the same widths for the HHLV configuration, averaged over all runs. The table shows the mean values, and the minimum and maximum interval ratios to indicate the spread due to different locations, and orientations as well as different noise realizations.

Parameter	AHLV / HHLV		A$_{45}$HLV / HHLV	
	$2\sigma\ width$	$std.\ acc$	$2\sigma\ width$	$std.\ acc$
M_c	$1.070^{+0.581}_{-0.326}$	$1.136^{+1.203}_{-0.463}$	$1.151^{+1.222}_{-0.453}$	$1.289^{+2.242}_{-0.493}$
η	$1.136^{+0.756}_{-0.496}$	$1.200^{+1.024}_{-0.529}$	$1.266^{+1.790}_{-0.699}$	$1.338^{+2.662}_{-0.638}$
t_c	$0.450^{+0.765}_{-0.421}$	$0.425^{+0.975}_{-0.400}$	$0.506^{+0.809}_{-0.478}$	$0.724^{+2.664}_{-0.704}$
d_L	$0.840^{+0.197}_{-0.137}$	$0.817^{+0.451}_{-0.345}$	$0.834^{+0.108}_{-0.137}$	$0.887^{+0.244}_{-0.332}$
α	$0.434^{+0.666}_{-0.423}$	$0.398^{+0.731}_{-0.393}$	$0.441^{+0.613}_{-0.427}$	$0.404^{+0.683}_{-0.397}$
δ	$0.228^{+0.380}_{-0.215}$	$0.194^{+0.325}_{-0.184}$	$0.247^{+0.275}_{-0.217}$	$0.199^{+0.319}_{-0.185}$
ι	$0.854^{+0.161}_{-0.192}$	$0.820^{+0.236}_{-0.507}$	$0.901^{+0.379}_{-0.168}$	$0.867^{+0.254}_{-0.253}$
ϕ	$1.000^{+0.010}_{-0.012}$	$0.986^{+0.073}_{-0.058}$	$1.000^{+0.011}_{-0.009}$	$0.989^{+0.104}_{-0.069}$
ψ	$1.039^{+0.149}_{-0.044}$	$1.014^{+0.117}_{-0.107}$	$1.029^{+0.181}_{-0.057}$	$1.031^{+0.273}_{-0.137}$
$\alpha - \delta$	$0.193^{+0.309}_{-0.172}$	—	$0.229^{+0.295}_{-0.157}$	—
$d_L - \iota$	$0.753^{+0.419}_{-0.305}$	—	$0.814^{+0.373}_{-0.422}$	—

Table 7 Errors ratios in the fit parameters. Comparative 2σ interval widths and standard accuracies for one dimensional probability distribution functions and comparative 2σ areas for two dimensional probability distribution functions (bottom two rows) averaged over all injections. All values for the AHLV and A$_{45}$HLV network configurations are given as fractions of the corresponding values for the HHLV network. The mean values of the ratios across all injections are computed; the error bars correspond to the spread between the minimum and maximum values of these ratios.

We should particularly point out the next-to-last line of the **Table 7**, α−δ row. The area of this 2-dimensional probability distribution function is a direct measure of the uncertainty in estimating the position of the source on the sky. The error box shrinks by a factor of ~ 3 - 5, similar to the improvements we found in the previous study and with timing.

Observe that the time-of-arrival of the signal at the center of the Earth improves by a factor of two in a four-site network as compared to a three-site network. This improvement is the reason why a four-site network has a greater sky resolution of the incoming gravitational wave signal. Moderate improvements are also seen in estimation of inclination and luminosity distance. However, the main point, as noted before, is that a four-site network gives one dimensional probability density functions that are unimodal. This is illustrated in **Figure 10**.

On the other hand, perhaps unexpectedly, the accuracy with which mass parameters are measured does not improve when we go from a three-site to a four-site network. We can speculate that the reason for this is that masses do not strongly correlate with extrinsic parameters (with the exception of the time of coalescence), so their estimation is not significantly improved by better sky localization or inclination measurements. On the other hand, the evolution of the phasing of the waveform is very sensitive to the masses—and the accuracy with which the phase can be measured by a given detector is sensitive to the SNR in that detector. Having two detectors at Hanford, which should see

identical signals (up to noise), effectively increases the SNR in that detector, potentially making better phase measurements possible. This may be the reason for the comparable or better measurement of chirp mass and mass ratio with the HHLV network configuration.

Given our limited statistics, the AHLV and A$_{45}$HLV network configurations appear to give comparable improvements to parameter-estimation accuracy. The sky localization appears to improve more with the A Australian detector than with the A$_{45}$ detector; however, this may not be statistically significant.

The large spread in the improvements in parameter-estimation accuracy for a network with an Australian interferometer (see the spread between minimum and maximum ratios for individual parameters in **Table 7**) may be indicative of the different effects of the network configuration on injections corresponding to particular choices of sky locations, inclinations, and orientations of the binary, rather than statistical fluctuations due to noise differences. However, we do not currently have a sufficiently dense grid of injections to test this hypothesis.
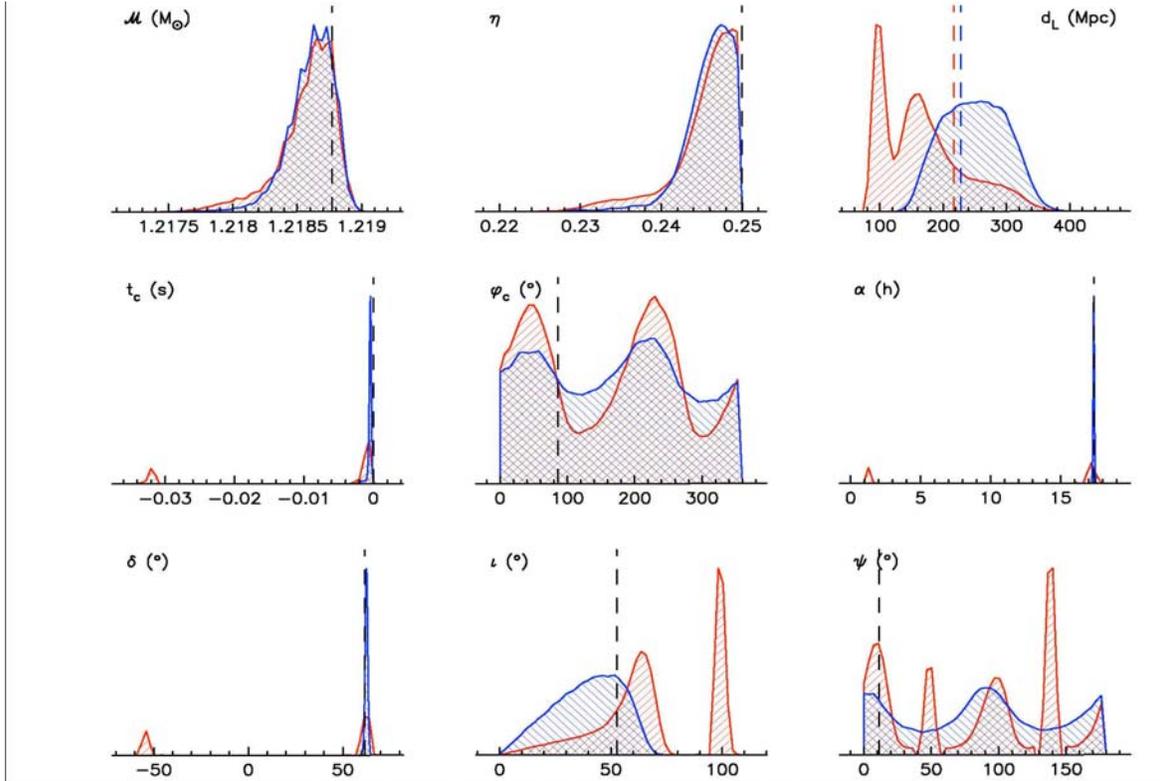
Figure 10 Comparison of the one-dimensional probability distribution functions for a typical source's parameters as detected by the HHLV (red) and AHLV (blue) networks. Note the bimodal posteriors in right ascension and declination for the HHLV vs the unimodal ones for the AHLV network. The latter network also allows for better estimates of the posteriors for inclination and luminosity distance. Dashed lines indicate the injected values (note that different injected values of the luminosity distance were used for the HHLV and AHLV so that the total network SNR is 15 in both cases).

The general conclusion of this study is that in a three-site network a number of parameters are strongly correlated with one another and, for certain regions of the parameter space, there is a strong degeneracy that makes parameter estimation quite

ambiguous. In fact, the posterior probability density functions of some of the parameters happen to exhibit a bimodal (and sometimes multi-modal) distribution. In a four-site network, most of the degeneracies are broken and the probability density functions tend to be uni-modal. For some of the parameters, like the luminosity distance and inclination angle, the variance in parameter estimation is the same for both networks. However, for AHLV there is generally no bias in the estimation of parameters. While the angular parameters and the luminosity distance improve qualitatively and quantitatively, the estimation of the chirp mass and mass ratio of the binary is literally the same in both AHLV and HHLV networks.

Robust Detection: False Alarm Rate
Unmodeled sources
We define a robust detection with a given network when the search volume V is sufficient to detect few GW events during the observation time with the significance greater than 5σ. The significance of the observation is determined by the false alarm rate achievable with the network. For example, if the rate of detection times the volume, RV>5, for a one year run, the network false alarm rate should be less that 1/5 per year using Poisson statistics. If the astrophysical rates are much lower (for example, RV ~ 0.5), then for robust detection the observation time should be much longer (~10 years) and the achievable false alarm rate should be much less (< 1/50 per year).

With the non-stationary and non-Gaussian data from the interferometers it will be difficult in a search for unmodeled bursts to obtain false alarm rates of less than 1/10 per year and simultaneously maintain the search volume of an ideal (Gaussian) network. **Figure 11** shows why. It is due to the tail of non-Gaussian background events for which the rate does not change much as the threshold on SNR increases.
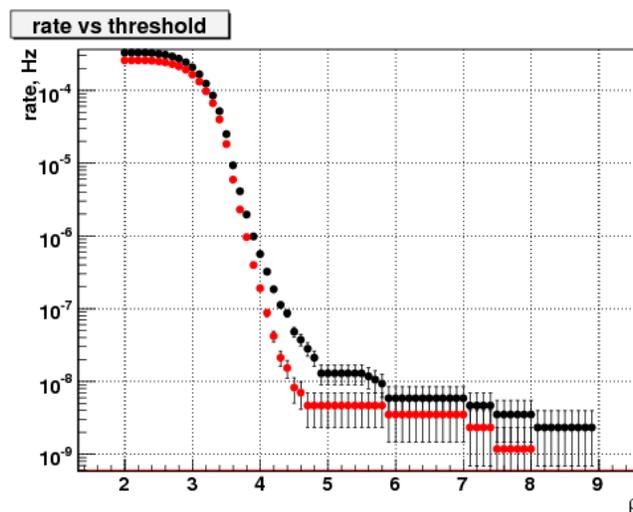
Figure 11 False alarm rate vs the correlated amplitude (proportional to SNR) for background triggers produced by the coherent waveburst algorithm in a search for unmodeled burst sources during the S6a run with the three detector HLV network. The black dots are for low frequencies (64-200Hz) and the red dots for high frequencies (200-2048Hz). The analysis was carried out with one week of data using 1000 time slides.
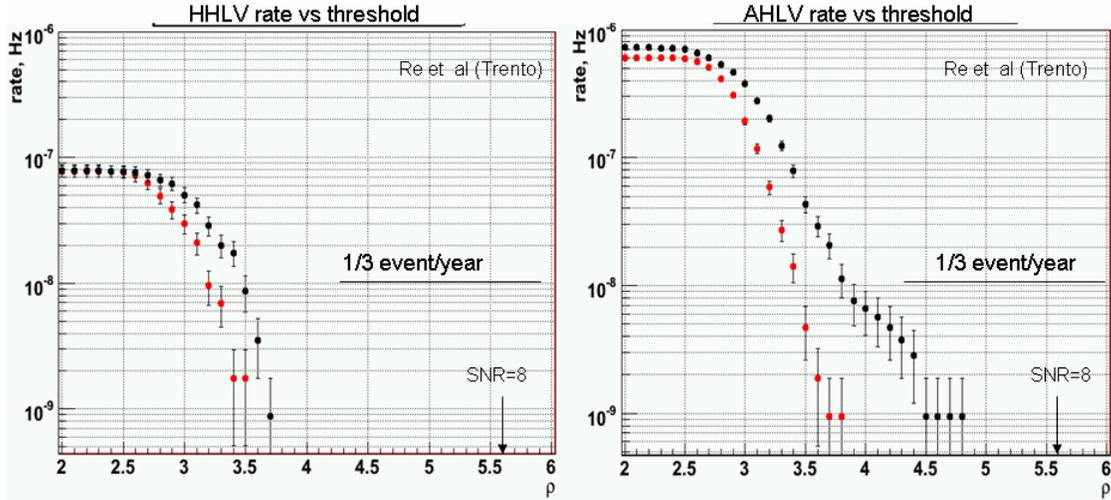
Figure 12 Background rate vs detection threshold for the two networks in a search for unmodeled burst sources. Black dots represent the low frequency band (64 -200Hz) and red dots the high frequency (200 – 2048 Hz) band. The significant change in the non-Gaussian tails relative to **Figure 11** is due to having four rather than three detectors in the network.

An estimate for the false alarm rate in burst searches with the advanced detectors for the AHLV and HHLV networks is shown in **Figure 12**. The analysis was carried out with the coherent wave burst algorithm. For both networks data collected during the S5/VSR1 and S6/VSR2 runs was used. During the S5 run two detectors were operational in Hanford H1 and H2, with H2 at half the sensitivity. To emulate a second advanced detector in Hanford, the H2 noise was rescaled to match the H1 sensitivity. To emulate the A detector, in the analysis we pretended that the rescaled H2 data stream originates from Australia. Most of the background events are produced by a random coincidence of noise transients in the detectors. To make the background estimates, the data streams were shifted by random time with respect to each other. In the HHLV network, because of the correlated noise between the two H interferometers, no time shifts were used for the H1H2 pair. In the AHLV network no correlation is expected between the A detector and the other detectors, therefore random time shifts were used between all detectors. To accumulate sufficient live time, a large number of the time shift configurations were used (~2000). The total accumulated background time was 36.4 years for the HHLV and 33.7 years for the AHLV networks.

In the analysis we used the likelihood method combining data from all detectors. Such a coherent approach takes into account the locations of the detectors, their antenna patterns and strain noise to reconstruct the individual detector responses as a function of sky coordinates. Since there is no true sky location associated with a random coincidence of noise transients, in most cases the reconstructed responses are inconsistent with each other, which helps to rule out many of the background events.

Figure 12 shows several important results. The first is the benefit derived from having a fourth detector in the network, best seen by comparing the change in the non-Gaussian tails between **Figure 11** and **12**. The second result, not obvious at the start of the study,

is that the two networks do not differ greatly in the false alarm rates associated with a range of SNR values. It had been guessed that the false alarm rate for the HHLV network could have been significantly less than that of the AHLV. The basis for this guess was the the idea that one could make a simple veto independent of sky location (allowing a small delay time) and polarization with signals from the two collocated detectors in the HHLV network and thereby provide a large reduction in the false alarm rate over the AHLV network. The modeling does not show this. The reason is that the coherent wave burst algorithm provides a similar but sky dependent veto for the AHLV network. This does a good job in reducing the long non-Gaussian tails by demanding consistency in the signals at the four detectors as it solves for the position on the sky. The high frequency data in **Figure 12** has come close to Gaussian while the low frequency data, which is considerably less stationary and initially more non-Gaussian, does show a difference between the networks. Additional modeling may demonstrate that there are benefits in detection confidence with the AHLV over the HHLV network because the unique position solutions provide more stringent consistency conditions on the signals.

Further modeling may show that the false alarm rate for AHLV is always a factor of a few larger than for the HHLV network (neglecting the correlations between H1 and H2). However, once the data remaining after the analysis approaches Gaussian, the difference becomes academic. In Gaussian data, the false alarm rate is a steep function of the threshold SNR. For example, at an SNR of 5, a few percent change makes an order of magnitude change in the false alarm rate. The key job for a detection algorithm used on non-Gaussian data originating in the instruments is to make the analyzed data as close to Gaussian as possible. A good example of the power of this statement is given in the next section of the report where the false alarm rates for modeled sources are dramatically reduced by a new analysis technique that removes the non-Gaussian tails.

Given the demonstrated power of the coherent network analysis, *the committee strongly urges the Compact Binary Coalescence search group to implement a coherent detection algorithm to be ready for the Advanced LIGO epoch.*

Issues surrounding first detections
The science case for LIGO South is based mainly on the desire for a network that yields the best science from a set of detected signals. Nevertheless, it is important to consider the issue of how we will achieve the first detections of gravitational wave signals. Given that the deployment of LIGO South would likely be delayed by as much as two years compared with the time for completion at the U.S. sites, a key question becomes, can we expect to detect signals with only the LHV network and at worst with only two U.S. interferometers?

The CBC group examined the extreme case: only two U.S. interferometers available. The examination consisted of study of the statistics of 0.43 years of time from the second year of S5, using data from H1 and L1, but not from either H2 or V1. Histograms of signals from the search for Binary Neutron Stars (i.e., chirp mass less that 3.48 Solar Masses) were made under a variety of conditions. By using 100 time slides to estimate background statistics, the question was asked whether the data was free enough of a non-Gaussian tail of glitches that a detection could be confidently made at SNR = 8. This is a

key issue, because estimates of Advanced LIGO range are based on the assumption that we will claim detections for signals with SNR of 8 or above.

The group examined the results at two levels of data quality, CAT2 and CAT3[3]. They also explored the use of two signal strength measures, SNR and the CBC group's scaled version called NewSNR. NewSNR reduces the SNR by a factor that grows as the chi-squared value grows. It produces a number that is very close to SNR for signals that match well the templates, but that can be dramatically reduced below the SNR if the chi-squared value is high (indicating bad match between signal and best-fitting template.)
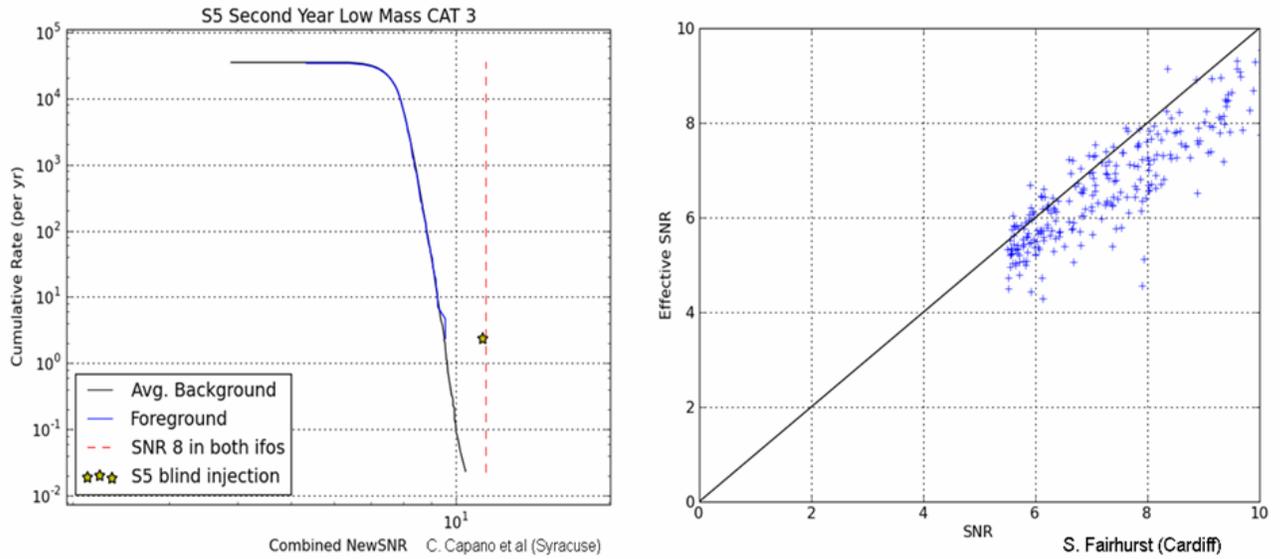
Figure 13 (Left) Rate of accidental detections with H and L detectors vs New SNR which includes a modification for the chi2. (Right) Shows the relation between the standard SNR and the newSNR for injections made during S5. The detection efficiency is not strongly affected by the use of the new SNR.

What was found is shown in **Figure 13(left).** Using the (chi-squared weighting) NewSNR and CAT3 vetoes, the histogram shows no sign of any non-Gaussian tail as far as this data set could reveal it, to a false alarm rate of about 0.03 per year. An artificial signal injected at about SNR 8 (NewSNR about 7.5) in each detector stands strongly above the background, making it easily detectable. Thus, the use of the signal-detection ranges based on a criterion of SNR = 8 seems eminently reasonable.

It is important to note that any relaxation of the chosen conditions introduces a non-Gaussian tail to the statistics that would call first signal detection into question. Use of SNR instead of NewSNR, use of only CAT2 vetoes, or use of the broader template set

---

[3] CAT2 and CAT3 are acronyms designating two different kinds of vetoes applied to the intereferometer output data. The CAT2 vetoes are indicators for bad data determined by straightforward criteria. The CAT3 vetoes are more subtle using statistical relations observed between the interferometer output data and many other channels monitoring the interferometer performance and the environment.

used to search for more massive binary systems, each produces a histogram with a substantial non-Gaussian tail, that could make it necessary to substantially raise the detection threshold. Thus, our prediction of successful detection at SNR = 8 with two detectors depends on having data quality not substantially worse in Advanced LIGO than in initial LIGO. Although not guaranteed, we think that this is a reasonable assumption for planning purposes.

The scaling between SNR and NewSNR for artificially injected signals is shown in **Figure 13(right).** At the benchmark value of SNR = 8, NewSNR is slightly below the value of SNR. This needs to be taken into account when comparing search results (that use NewSNR) with theoretical range predictions that use SNR. However, the difference is small and well paid back by the elimination of the non-Gaussian tail in the accidental event rate.

References

"Bayesian Coherent Analysis of In-Spiral Gravitational Wave Signals with a Detector Network" J. Veitch and A. Vecchio, Phys Rev D V81 062003 (2010)

"Geometrical Expression for the Angular Resolution of a Network of Gravitational-Wave Detectors" L. Wen and Y. Chen, LIGO Document P1000017-v3, Feb 8, 2010.

"Detection, Localization and Characterization of Gravitational Wave Bursts in a Pulsar Timing Array" L.S.Finn and A.N. Lommen, arXiv: 1004,3499
(2010) submitted to Ap.J

" Constraint Likelihood Analysis for a Network of Gravitational Wave Detectors "
 S. Klimenko, S. Mohanty, M Rakhmanov, G. Mitselmakher Phys Rev D V72 122002 (2005)

Appendices

Initial LIGO rationale for H1 and H2

The idea that one could multiplex the beam tubes with several interferometers of both full and half length arms was incorporated in the initial LIGO proposal made to the NSF in 1989. With final approval of initial LIGO, the decision was made to construct the minimum configuration, initially consisting of 4km interferometers at both sites with a 2km at Hanford. To not preclude additional instruments later, the buildings at Hanford were designed to allow both two 4km and one 2km while those at Livingston to accommodate two 4km instruments.

The motivation for the 2km interferometer at Hanford was to:

1. Provide an additional detector to reduce the accidental coincidence rate for gravitational waves in the face of both Gaussian and non-Gaussian noise. It was recognized that there would be some correlation between the 4km and the 2km from environmental noise, nevertheless, the ability to veto events observed in the main 4km detectors was the key function.

2. Provide an additional consistency test for candidate gravitational wave events through the amplitude ratio proportionality with length between the 2 and 4km detectors. It was recognized that the value of the consistency test would be a strong function of the signal to noise of the gravitational wave signals.

3. Provide diagnostics for a variety of environmental perturbations observed in the main interferometer output that could then be eliminated with further development of the detector and facilities.

Not all of the initial precepts have been realized during the LIGO science runs. The amplitude and waveform consistency tests were very valuable, especially in burst searches, until Virgo brought us a third interferometer site without the potential noise correlations and with less of an intrinsic limit on interferometer sensitivity. Since the most likely detection candidates are expected to have low signal to noise, a twofold sensitivity compromise is a large price to pay. Also, in practice the correlated noise sources identified to date have tended to be at points in the corner station that lacked the very high seismic and acoustic isolation of the core optics chambers; thus sharing the same corner station appears to have overwhelmed any advantage of not sharing common end stations.

The baseline network for the Advanced LIGO program is to move the 2km detector at Hanford to a length of 4km. This does not remove the correlations between the detectors but does make the detectors at Hanford comparable in sensitivity.

Committee Charter

DATE: January 4, 2010

TO: Sam Finn, Peter Fritschel, Sergei Klimenko, Fred Raab, Bangalore Sathyaprakash, Peter Saulson, Rai Weiss (chair)

FROM: Jay Marx, Albert Lazzarini, David Reitze

SUBJECT: LIGO South Scientific Evaluation Committee

Refer to: LIGO- M1000003-v1

Funding limitations in Australia are such that the possibility of building an Australian interferometer is essentially non-existent without substantial in-kind support from the international gravitational wave community. Thus, LIGO Laboratory is very seriously considering the possibility of offering one of the Advanced LIGO interferometers slated for installation at Hanford for alternate installation at a suitable location/facility in Australia.

From a scientific standpoint, a third Advanced LIGO interferometer in Australia together with the Advanced Virgo interferometer in Italy would constitute a larger global worldwide network, with four comparably sensitive interferometers distributed worldwide. While the feasibility of a move depends on many factors that go beyond purely scientific motivations, the decision must rest ultimately on an objective evaluation of the astrophysics gains that come from having a third LIGO interferometer located in Australia as opposed to the current baseline of having two collocated interferometers at Hanford.

We ask you to serve on an evaluation committee whose charge is to compare the scientific benefits of relocating the third Advanced LIGO interferometer to Australia against those of maintaining two interferometers at Hanford. Fundamentally, the question to be addressed is "How much more gravitational wave astronomy could be enabled by moving an interferometer to Australia?" The charge should be viewed in the context of our expectations that i) once they are operating at design sensitivity, the Advanced LIGO and Virgo detectors will go beyond detections and usher in the era of gravitational wave astronomy, and ii) the Advanced LIGO and Virgo detectors will have a scientific lifetime extending through 2030 and possibly beyond.

Consider the charge as broadly as possible, and quantitatively to the extent possible. Specific issues which should be studied include, but are not limited to:

- What new astrophysics is enabled by placing an interferometer in Australia? Generally, how might gravitational wave astronomy evolve over a twenty year time scale by installing an interferometer in Australia when compared with leaving both interferometers at Hanford?

- Consider what impact a move would have on the science goals in the Advanced LIGO era. Specifically, how might each of the search groups' science goals be enhanced or diminished with such a move?
- Assuming no detections in S6/VSR2, would relocating an interferometer have a positive or negative effect on the time to a first detection?- With two co-located tunable interferometers, it is possible to separately tailor each of their sensitivities, for example, to effectively provide a broader bandwidth in a single location or to search for a specific pulsar. Would any science be compromised by losing the capability of doing this at a single site? (Presumably the third Advanced LIGO detector could be operated in narrowband regardless of its location.)
- What impact would the loss of co-located interferometers have on background suppression for transient burst and inspiral searches?
- What advantages would a move have on multi-messenger (joint GW-EM and GW- neutrino) searches? (e.g. in sky localization vs SNR; in sky coverage, etc.)
- Assuming that the interferometer would be located at Gingin near Perth, what would be the preferred orientation of an Australian interferometer?
- What impact would installing an interferometer in Australia have on GW source parameter estimation (eg, polarization analysis)? Are there any disadvantages?

Note that we are not asking you to address construction, commissioning, operations, or management issues in this study. However, you should comment upon these or any other issues to the extent that they influence the primary scientific considerations.

The final report, not more than 10 pages, should be delivered by April 15, 2010. A preliminary report should be provided to the LIGO Directorate by March 15. Your report should not make any endorsements, but should clearly state the positive and negative scientific consequences of installing an Advanced LIGO interferometer in Australia. If needed, feel free to consult with others in developing the report, but please keep the Directorate informed of whom else is being consulted.